

How do ocean warm anomalies favor the aggregation of deep convective clouds?

Sara Shamekh*

*Laboratoire de Météorologie Dynamique/IPSL, École Normale Supérieure, PSL Research
University, CNRS, Paris, France*

Caroline Muller

*Laboratoire de Météorologie Dynamique/IPSL, École Normale Supérieure, PSL Research
University, CNRS, Paris, France*

Jean-Philippe Duvel

*Laboratoire de Météorologie Dynamique/IPSL, École Normale Supérieure, PSL Research
University, CNRS, Paris, France*

Fabio D'Andrea

*Laboratoire de Météorologie Dynamique/IPSL, École Normale Supérieure, PSL Research
University, CNRS, Paris, France*

*Corresponding author address: Laboratoire de Météorologie Dynamique, École Normale
Supérieure, 24 Rue Lhomond, 75005 Paris, France
E-mail: shamekh@lmd.ens.fr

ABSTRACT

18 We investigate the role of a warm sea-surface temperature (SST) anomaly
19 (hot-spot of typically 3 K to 5 K) on the aggregation of convection using cloud
20 resolving simulations in a non-rotating framework. It is well known that SST
21 gradients can spatially organize convection. Even with uniform SST, the spon-
22 taneous self-aggregation of convection is possible above a critical SST (here
23 295 K), arising mainly from radiative feedbacks. We investigate how a cir-
24 cular hot-spot helps organize convection, and how self-aggregation feedbacks
25 modulate this organization. The hot-spot significantly accelerates aggrega-
26 tion, particularly for warmer/larger hot-spots, and extends the range of SSTs
27 for which aggregation occurs, however at cold SST (290 K) the aggregated
28 cluster disaggregates if we remove the hot-spot. Large convective instabil-
29 ity over the hot-spot leads to stronger convection and generates a large-scale
30 circulation which forces the subsidence drying outside the hot-spot. Indeed,
31 convection over the hot-spot brings the atmosphere towards a warmer tem-
32 perature. The warmer temperatures are imprinted over the whole domain
33 by gravity waves and subsidence warming. The initial transient warming
34 and concomitant subsidence drying suppress convection outside the hot-spot,
35 thus driving the aggregation. The hot-spot induced large-scale circulation can
36 enforce the aggregation even without radiative feedbacks for hot-spots suffi-
37 ciently large/warm. The strength of the large-scale circulation, which defines
38 the speed of aggregation, is a function of the hot-spot fractional area. At equi-
39 librium, once the aggregation is well established, the moist convective region
40 with upward mid-tropospheric motion, centered over the hot-spot, has an area
41 surprisingly independent of the hot-spot size.

42 **1. Introduction**

43 In the tropics, convection can be organized by synoptic dynamical systems such as equatorial
44 waves or tropical depressions, but it may also have its own organization sources such as in squall
45 lines, or more generally in mesoscale convective systems. Organized convection is associated with
46 extreme weather conditions (Houze 2004), and can strongly impact the hydrological cycle and the
47 top-of-atmosphere radiation budget (Tan et al. 2015; Tobin et al. 2012). For large-scale processes
48 such as the Madden Julian Oscillation, the aggregation of the convection may generate non-linear
49 effects modifying the average circulation at basin scale (Bellenger et al. 2009). However, the
50 physical processes responsible for the mesoscale organization of convection are still not clearly
51 identified and are typically not specifically accounted for in global climate models (GCMs) (Mapes
52 and Neale 2011).

53 The spontaneous clustering of convective clouds in simulations in idealized settings, typically
54 non-rotating Radiative-Convective Equilibrium (RCE), provides a manageable framework to gain
55 fundamental understanding of the physical processes at stake. Non-rotating RCE is an idealization
56 of the tropical atmosphere where the Earth's rotation is neglected, a reasonable approximation in
57 the deep tropics where the Coriolis parameter is small, and where the large-scale circulation (larger
58 than the model domain) is neglected. In other words, in RCE, there is no advection of energy into
59 or out of the domain. Thus in the domain mean, surface latent and sensible heat fluxes are in
60 balance with the net radiative cooling of the atmosphere (top-of-atmosphere minus surface).

61 In the tropics, such equilibrium is only reached at large, thousands of kilometers scales (Muller
62 and O’Gorman 2011). The idealized framework of RCE has proven to be useful to study and
63 improve our understanding of numerous aspects of tropical convection, including precipitation
64 extremes (Muller et al. 2011; Muller 2013), entrainment (Romps 2010), cold pools (Tompkins

2001a), atmospheric thermodynamics (Pauluis and Held 2002) or rain evaporation (Muller and Bony 2015). Notably, it has led to the discovery of the remarkable ability of deep convection to spontaneously cluster in space despite homogeneous forcing in cloud-resolving models (CRMs). These are models with sufficient kilometric horizontal resolutions to resolve the main features of deep convection, instead of parameterizing them.

Typical RCE simulations with homogeneous forcing (doubly-periodic geometry, square domain, constant sea-surface temperature (SST) in space and time) reach a statistically steady state in which convection and clouds are somewhat randomly distributed. But under certain conditions, including large domains, deep clouds aggregate into a region of the domain, surrounded by a dry environment devoid of deep convection. This phenomenon, known as self-aggregation in the literature (see, e.g., Wing et al. (2017) for a review), leads to an equilibrium state with dry and warm mean thermodynamic profiles, and enhanced outgoing longwave radiation (OLR) to space (Bretherton et al. 2005; Tobin et al. 2012). Since its discovery in idealized CRM simulations, the self-aggregation of deep convection has been confirmed to occur in more realistic settings (Holloway 2017) and even in GCMs with parameterized convection (Coppin and Bony 2015).

Radiative feedbacks are believed to be key for self-aggregation, at least at temperatures observed in the tropical atmosphere (Wing et al. 2017). It is the circulation generated by the differential longwave radiative cooling rates between dry (strong cooling) and moist (little cooling or even warming) regions which is believed to trigger and maintain the convective aggregation (Bretherton et al. 2005; Muller and Held 2012). Strong cooling in dry regions yields subsidence down to low levels, and a near-surface flow from dry to moist regions. Such a process was already proposed by Gray and Jacobson (1977) to explain the observed reinforcement of large convective systems at the end of the night. This circulation transports near-surface high moist static energy (MSE) from dry to moist regions. This MSE upgradient transport maintains high MSE in the moist region,

89 helping to maintain deep convection there. In fact, in the CRM used in this study (System for
90 Atmospheric Modeling, or SAM (Khairoutdinov and Randall 2003)), there is no self-aggregation
91 without interactive radiation (unless the evaporation of rain is artificially suppressed (Muller and
92 Bony 2015), a particular case which will not be discussed here). Because of the idealized settings
93 in which self-aggregation was discovered, its relevance to the real world is still debated. Notably,
94 the aforementioned CRM studies used spatially and temporally constant and uniform sea-surface
95 temperatures (SSTs).

96 The impact of SST anomalies on deep convection has already been widely studied in the lit-
97 erature (Tompkins 2001b; Kuang 2012; Ramsay and Sobel 2011; Sobel and Bretherton 2000).
98 Tompkins (2001b) found in particular that flipping the SST anomaly leads to migration of the
99 convective clusters over the warm anomaly. The migration of aggregated convective cluster over
100 warm anomaly has been confirmed by other studies which used a slab ocean in order to have in-
101 teractive SST (Coppin and Bony 2015; Grabowski 2006). Using a single column model (SCM)
102 and CRM, Ramsay and Sobel (2011) and Wang and Sobel (2011) showed that precipitation rate
103 increases over local warm SST and is determined by the temperature anomaly rather than by the
104 mean SST. Daleu et al. (2017) confirmed this result using two adjacent SCMs with different SST.
105 The SST difference, if large enough, can suppress convection in the cold column and strengthen it
106 in the warm column. Notably, SST gradients can generate a large-scale circulation that can lead to
107 a migration of deep convection towards the warmest SST.

108 Another type of surface temperature anomalies are tropical islands with different surface proper-
109 ties, which act as a surface forcing and change the intensity of convection (Crook 2001; Beringer
110 and Tapper 2002) and thermal structure of the atmosphere (Cronin et al. 2014). Rainfall over
111 tropical islands is larger than over the surrounding ocean (Cronin et al. 2014; Sobel et al. 2011;
112 Qian 2008; Wang and Sobel 2017), however the strength of the thunderstorms and precipitation

113 depends on several factors such as the size of the islands, wind speed and direction and the island's
114 topography (Wang and Sobel 2017; Crook 2001). Convective events over tropical islands show
115 large diurnal variations, however they build up an average ascent (Cronin et al. 2014) .

116 Ocean mesoscale eddies (Chelton 2011) can also be associated with SST anomalies reaching a
117 few degrees in cold core cyclonic eddies or warm core anticyclonic eddies. These persistent ocean
118 eddies have typical radius varying with latitude, from a hundred to a few hundreds of kilometers in
119 the tropics ($\pm 20^\circ$ latitude), to around 50 km or less in mid-latitudes. As a surface forcing, eddies
120 can impact the atmosphere locally (Sugimoto et al. 2017) by enhancing low level convergence and
121 thus convective precipitation. Potentially, the eddies changes the cloudiness and wind field which
122 can impact the large scale circulation .

123 Whether and how such persistent SST anomalies, as an external forcing, can favor or suppress
124 the aggregation of convection is, to our knowledge, still not well covered in the literature. In this
125 paper, we investigate the aggregation response to an idealized, circular SST anomaly referred to
126 as a “hot-spot”. We must emphasize that the aggregation forced by a hot-spot, when it is the case,
127 is not anymore ”self-aggregation” but rather a forced aggregation. Of particular interest are the
128 following questions:

- 129 • How does the presence of an ocean hot-spot modify or enforce the aggregation process of
130 the deep convection? And how does this modification depend on the hot-spot radius and
131 temperature anomaly?
- 132 • How does the hot-spot impact the large-scale circulation?
- 133 • In the presence of a hot-spot, how does the aggregation physics differ from the self-
134 aggregation ones; specifically, does aggregation disappear in the absence of radiative feed-
135 backs (known to be crucial for self-aggregation over homogeneous SST)?

136 The next section, § 2, describes the cloud-resolving model used and the experimental setup, as
 137 well as the metrics used to measure (self-)aggregation. § 3 investigates the impact of the hot-spot
 138 on convective aggregation, and the sensitivity to hot-spot properties. § 4 investigates whether ra-
 139 diative feedbacks are still necessary for aggregation to occur when a hot-spot is present. Addition-
 140 ally, we derive a simple, two-box model to help comparison between the onset of self-aggregation
 141 and aggregation. In § 5 we briefly discuss the equilibrium phase, once aggregation has occurred.
 142 Conclusions are given in § 6.

143 2. Model description and simulation design

144 *a. Cloud-resolving model*

145 The CRM used is the model System for Atmospheric Modeling (SAM) version 6.11.1 (Khairout-
 146 dinov and Randall 2003). This model solves the anelastic equations of conservation of momentum,
 147 water (with 6 species present in the model, water vapor, cloud liquid, cloud ice, precipitating rain,
 148 precipitating snow, and precipitating graupel), and energy. The relevant energy for moist con-
 149 vection is the moist static energy, as it is conserved (approximately, i.e. neglecting viscous and
 150 subgrid-scale effects) under adiabatic processes including the phase change of water. More pre-
 151 cisely in this model, the so-called "frozen" MSE is conserved during moist adiabatic processes,
 152 including the freezing of precipitation. The frozen MSE is given by

$$MSE = c_p T + gz + L_v q_v - L_f q_{ice}, \quad (1)$$

153 with the specific heat capacity of air at constant pressure c_p , temperature T , gravity g , height z ,
 154 latent heat of evaporation L_v , water vapor mixing ratio q_v , latent heat of fusion L_f , and mixing
 155 ratio of all ice phase condensates q_{ice} .

156 The subgrid-scale turbulence is modeled using a Smagorinsky-type parameterization, and we
157 use the 1-moment microphysics formulation, following Bretherton et al. (2005) and Muller and
158 Held (2012). Bulk formulae are used to compute surface fluxes. Further information about the
159 model can be found in Khairoutdinov and Randall (2003).

160 Most simulations use interactive radiation, using the radiation code from the National Center for
161 Atmospheric Research (NCAR) Community Atmosphere Model version 3 (CAM3; (Collins et al.
162 2006)). For simplicity, we neglect the diurnal cycle and use the daily mean incoming solar insola-
163 tion of 413 W m^{-2} (same setting as Tompkins and Craig (1998)). Studies of self-aggregation over
164 the ocean with a diurnal cycle show that, quantitatively, a diurnal cycle can change the strength of
165 the hydrological cycle, increasing the daily precipitation range. But qualitatively, beyond this daily
166 modulation of amplitude, it does not seem to affect the fact that deep convection self-aggregates
167 or not.

168 In some simulations, radiative feedbacks are turned off by homogenizing radiative cooling rates
169 horizontally, at each height and time step, following Muller and Held (2012). Note that in that
170 case, the domain average radiative cooling rates can still evolve in time.

171 *b. Experimental setup*

172 The model domain is square, doubly-periodic in both horizontal directions x and y . We run
173 simulations with two domain sizes, $(288 \text{ km})^2$ and $(576 \text{ km})^2$ (except for one simulation shown in
174 Figure 1 with a smaller $(96 \text{ km})^2$ domain). The horizontal resolution is 3 km and the vertical grid
175 spacing increases gradually with height, with the first level at 25 m and a resolution of 50 m close
176 to the sea surface, reaching a vertical resolution of 500 m in the mid troposphere. There are 64
177 vertical levels which span 27 km in the vertical. This includes a sponge layer in the upper third of
178 the domain (from $z = 18 \text{ km}$ to 27 km) where the wind is relaxed to zero in order to reduce gravity

179 wave reflection and buildup. No large-scale forcing or wind is imposed. We neglect the Earth's
180 rotation, a reasonable approximation in the tropics where the Coriolis parameter is small.

181 The initial conditions for the different mean SSTs (horizontal mean SSTs in our simulations with
182 and without hotspot) are obtained from a smaller domain run with the corresponding SST at RCE
183 $((96 \text{ km})^2$ run to 50 days), then using time and domain averaged profiles of the last 5 days. We
184 run two different types of simulations: simulations with a uniform and constant sea surface tem-
185 perature that we refer to as ocean experiments, and simulations with a warm temperature anomaly
186 referred to as hot-spot experiments. The hot-spot is a circular area with a higher temperature than
187 the surrounding ocean, located at the center of the domain. A given hot-spot simulation will be
188 defined by its temperature anomaly dT and its radius R so that, for example, simulation $dT5R60$
189 is for a hot-spot with a temperature anomaly of 5 Kelvin and a radius of 60 km. The upper two
190 panels of Figure 1 shows snapshots of near-surface air temperature and cloud water for two sim-
191 ulations with a different domain size and hot-spot radius. This illustration shows that, although
192 there is some organization of convection on the small domain in the presence of a hot-spot, the
193 self-aggregation of convection surrounded by extremely dry air only occurs in the large-domain
194 simulation. This is well captured by the metrics used to quantify the degree of aggregation de-
195 scribed next and shown in Figure 1c. In the following, in both ocean and hot-spot experiments, we
196 also investigate the role of radiative feedbacks by repeating some simulations with homogenized
197 radiation.

198 *c. Aggregation metrics*

199 The convective aggregation is associated with progressive drying of the dry environment sur-
200 rounding deep clouds, and progressive moistening of the moist region where deep convection
201 occurs. This leads to increased horizontal moisture variability. Thus a common index for self-

aggregation is the difference between the 75th and 25th percentiles of precipitable water, ΔPW_{75-25} (Muller and Held 2012; Muller and Bony 2015). Since here we will compare simulations with different SSTs, we will use precipitable water normalized by the saturation water vapor path, i.e. we will use column relative humidity CRH (Wing and Cronin 2016),

$$CRH = \frac{\int q_v \rho dz}{\int q_{v,sat} \rho dz}, \quad (2)$$

where $q_{v,sat}$ denotes the saturation water vapor mixing ratio, ρ density and the vertical integration is done over the troposphere. Our aggregation index is the difference between the 75th and 25th percentiles of column relative humidity, ΔCRH_{75-25} . Figure 1 illustrates the increase of this index (bottom panel) in the simulation that aggregates (middle panel).

In SAM, self-aggregation has been shown to start with the strengthening and the expansion of a dry patch, becoming drier and larger. This dry region, devoid of deep convection, was sometimes referred to as the “radiative dry pool” (Coppin and Bony 2015; Zuidema et al. 2017), as it is believed to be radiatively driven. The dry patches are thus of primary importance, as the self-aggregation of convection can eventually result from the confinement of the deep convection in a restricted region because of the expansion of a dry patch in our doubly-periodic geometry. In the following, the dry patch is defined as the area where the CRH is below the 25th percentile.

3. Hot-spot impact on aggregation of deep convection

Here, we first investigate how the presence of a hot-spot impacts the aggregation of convection in the presence of radiative feedbacks. Of particular interest is whether the aggregation is faster, and whether the deep convection area ends up being localized over the hot-spot.

222 *a. Results without and with hot-spot at different SSTs*

223 The upper row of Figure 2 shows the *CRH* maps in a control ocean experiment with a mean
224 SST of 300 K at different times started from homogeneous conditions. We observe the typical
225 evolution of self-aggregation: the appearance of a dry patches after a few days (day 11) and thus
226 the extension and merge of these dry patches into a single patch (day 31). At day 41, the *CRH*
227 in the dry region reaches extremely low values, and convection and moisture are confined to a
228 small part of the domain. After day 41, the moist patch shrinks to narrow region surrounded by a
229 very dry environment. The increased spatial moisture variability between dry and moist regions,
230 largely due to enhanced drying, is also visible in ΔCRH_{75-25} (Figure 3a). It increases up to day
231 40 and then starts to decrease slowly. With further progress of aggregation, the high CRH region
232 shrinks to a circular area smaller than 25 percent of the domain, thus *CRH*₇₅ decreases, leading to
233 the decrease of the aggregation index.

234 Self-aggregation over fixed SST is known to depend on the domain mean SST. Using the same
235 SAM model, Wing and Emanuel (2014) find that warm SSTs favor aggregation, while Coppin and
236 Bony (2015) find in a GCM that self-aggregation is surprisingly favored both for SSTs larger than
237 295K or smaller than 285K. In very cold snowball simulations, aggregation can also occur (Abbot
238 2014), though in that case a weak wind shear can prevent the aggregation. The exact relation
239 between an average SST and the self-aggregation response is hence still unclear, but the general
240 consensus is that self-aggregation is favored at warm SSTs (Emanuel et al. 2014). Consistently,
241 we find that for a colder SST of 290 K aggregation does not occur, and that the aggregation speed
242 increases regularly with the SST for SST values between 295 K and 305 K (Figure 3a).

243 Simulations with the same mean SST, but with different hot-spot characteristics are performed
244 to analyze the role of the SST anomaly on the convective aggregation. Here the domain-mean

245 SST is kept constant at 300 K in order to isolate the effect of the hot-spot temperature anomaly.
246 Consequently, the surrounding ocean temperature is slightly lower than 300 K in the hot-spot
247 simulations. However, it has been argued in previous studies (Ramsay and Sobel (2011); Wang
248 and Sobel (2011)) that the control parameter is the SST anomaly (dT) and not the absolute SST,
249 at least for a reasonable temperature change. Figure 2b shows the hot-spot experiment dT5R60
250 ($dT=5$ K and $R=60$ km). Spatially, the main aspects of aggregation in the presence of a hot-spot
251 are similar to the ocean experiment, with a progressive expansion of dry regions. The aggregation
252 is however much faster with the hot-spot and the convection is eventually organized over or near
253 the hot-spot. Note that the location of the aggregation is not stable, and whether the aggregated
254 convective cluster stays over the hot-spot depends on hot-spot radius and temperature. If the hot-
255 spot is sufficiently large and/or warm, it sustains the convective cluster over it, otherwise, it does
256 not necessarily stay over the hot-spot after its formation. We will discuss this in more detail in § 5.

257 Looking at the aggregation index (Figure 3b), the maximum aggregation is in fact reached after
258 only 10 days in dT5R60 compared to 40 days in the ocean simulation at 300K. Thus, the presence
259 of a hot-spot may accelerate the aggregation by a factor of 4. However the aggregation is much
260 faster with a hot-spot, when the aggregation is fully reached, the aggregation index is fairly com-
261 parable between the simulations with and without a hot-spot. The hot-spot temperature anomaly
262 plays a significant role in accelerating or enforcing the aggregation, as can be seen on Figure 3b.
263 For dT5R60 the aggregation index reaches a maximum after only 10 days while for dT3R60 the
264 maximum is reached in 20 days. Thus, the aggregation speed is favored by larger hot-spot tem-
265 perature anomaly. The hot-spot size also plays a role with a maximum aggregation index reached
266 in less than 10 days for dT3R120. Therefore, the larger the hot-spot, the faster the aggregation.
267 Note though that for very large hot-spots relative to the domain size (see below), this can not hold
268 anymore. A hot-spot can also extend the range of SSTs for which an aggregation occurs. For

example, with an average SST of 290 K, there is no self-aggregation for uniform SST (3a), but the dT5R60 experiment at 290 K aggregates even faster than uniform ocean simulations at 305 K. (3b).

b. Development of a large-scale circulation

Here, we hypothesize that the presence of the hot-spot favors and accelerates the formation of a large-scale circulation that triggers the onset of convective aggregation, and thus extends the range of SSTs at which aggregation occurs.

To explain the acceleration of aggregation with a hot-spot, we look at virtual potential temperature (θ_v) anomaly. In the free troposphere, gravity waves remove horizontal θ_v anomalies very efficiently (Bretherton and Smolarkiewicz 1989; Ruppert and Hohenegger 2018) so that θ_v profile above the boundary layer is fairly uniform over the domain especially when it is averaged over a few hours. So the main source of instability is the buoyancy anomaly in the boundary layer. Figure 4 shows θ_v anomaly averaged over the boundary layer for ocean experiment at SST=300 K at day 31 and hot-spot experiment dT5R60 with mean SST equal to 300 K at day 11 (Figure 2 shows the CRH evolution for these two simulations). We compare these two days as the aggregation index and the fraction of area covered with low (high) CRH are comparable between the two simulations. In general there is a positive θ_v anomaly in moist areas (except directly below clouds where cold pools result from the partial evaporation of rain), that enforces convergence of low-level air toward the moist area. Consistent with the faster aggregation, the θ_v anomaly is larger over the hot-spot. θ_v depends on both temperature and water vapor. In both the ocean and hot-spot simulations, the moisture contribution to the θ_v anomaly in moist regions is positive. But the temperature contribution is smaller in the ocean experiment. In the hot-spot simulations, over the hot-spot, both temperature and moisture have a positive contribution to θ_v resulting in a slightly larger θ_v .

292 anomaly and a stronger instability over the hot-spot that leads to stronger convection.

293 The corresponding pressure gradient at the first few levels enforces a convergence of moisture
294 toward the moist region. With a hot-spot, the pressure gradient is larger and it stays over the hot-
295 spot. This convergence favors convection over the hot-spot by transporting low level moist air and
296 by providing energy to lift the air above the hot-spot. Additionally, the convergence of moisture
297 removes moisture from the environment and inhibits convection there. This process (low-level
298 transport of moisture toward the moist region) thus seems common to both self-aggregation and
299 aggregation but is stronger in the latter case. There is a difference though: in aggregation with a
300 hot-spot, it is the strength of the upward mass flux over the hot-spot which seems to control the
301 large-scale circulation and thus the aggregation speed. Ascent over the hot-spot forces compensat-
302 ing subsidence in the environment, which dries the troposphere and results in further suppression
303 of convection there and enhancement of moisture transport toward the hot-spot. This upward
304 motion over the hot-spot and thus subsidence in the environment, is partly a consequence of our
305 period boundary conditions, and it builds up a large scale circulation that accelerates the aggrega-
306 tion. Instead, with self aggregation, it has been hypothesized that it is the subsidence in dry regions
307 which initiates and controls the large-scale circulation, and thus the self-aggregation speed. This
308 development of a large-scale circulation will be further investigated in the next section.

309 A natural question then, is whether the large-scale circulation enforced by the hot-spot can be
310 maintained even in the absence of hot-spot, solely by internal self-aggregation feedbacks. The
311 sensitivity of self-aggregation to initial conditions is well documented. Aggregated states that are
312 imposed as initial conditions can persist, even under conditions which do not favor the sponta-
313 neous self-aggregation from homogeneous initial conditions (Khairoutdinov and Emanuel 2010;
314 Muller and Held 2012). To investigate whether the hot-spot aggregation exhibits hysteresis, we re-
315 peat the dT5R60 with SST=290 K simulation, which does not self-aggregate without hot-spot, for

316 30 days, and then remove the hot-spot (by simply setting dT to zero) and run for another 30 days.
317 The aggregated cluster spreads over the domain and disaggregates. Therefore the aggregation is
318 not maintained without the hot-spot in this case.

319 **4. Convective aggregation without radiative feedbacks**

320 *a. Hot-spots with or without radiative feedbacks*

321 Radiative feedbacks have been shown by many studies to be necessary for convective self-
322 aggregation, at least for typical tropical SSTs around 300 K (Wing et al. 2017). The balance
323 between radiative cooling and subsidence warming in dry regions (Mapes 2001) creates a posi-
324 tive feedback that results in radiatively enhanced subsidence and drying of already dry regions.
325 Sensitivity studies show that removing radiative feedbacks, by homogenizing radiative cooling
326 rates, prevents the self-aggregation. Here we test the occurrence of aggregation without radiative
327 feedbacks in hot-spot experiments, listed in Table 1.

328 Comparing the dT5R60 simulation with (Figure 2b) or without (Figure 5a) radiative feedbacks,
329 we see that homogenizing the radiation prevents aggregation for a hot-spot radius of 60 km. How-
330 ever, increasing the hot-spot radius to 70 km (Figure 5b) yields aggregation even without radiative
331 feedback. For $R=70$ km, the aggregation is very slow, but it becomes much faster at larger radius
332 (Figure 6). It is worth noting that simulations with $R=70$ and 80 km give a banded aggregation.
333 For larger hot-spots, a circular aggregation of the convection develops in a few days, with a max-
334 imum aggregation index reached in less than 10 days with $R=180$ km. This is fast compared to
335 typical overturning time scale of the atmosphere (Grabowski and Moncrieff 2001), suggesting that
336 the circulation between dry and moist regions is greatly accelerated by the presence of the SST
337 anomaly. By reducing this anomaly to 3K instead of 5K, there is no convective aggregation, even

338 for a radius of 80 km (Figure 6). A persistent SST anomaly can thus clearly trigger a convective
339 aggregation in SAM, even without radiative feedbacks. This aggregation requires a minimum size
340 and amplitude of the SST anomaly, and is faster for warm and large hot-spots. In order to clarify
341 the physical processes responsible for convective aggregation in that case, we look in the next
342 section at the large-scale circulation in more detail, in particular the subsidence in the dry regions.

343 Note that because we keep the mean SST constant, changing the hot-spot radius R and temper-
344 ature anomaly dT , also changes the temperature outside the hot-spot and the absolute temperature
345 of the hot-spot (both reduced to keep the domain mean SST constant). To verify that the lead-
346 ing order parameter determining the onset and speed of aggregation is the hot-spot temperature
347 anomaly dT , not its absolute temperature, we redo some of the simulations keeping the tempera-
348 ture equal to 300 K outside the hot-spot, and simply adding a hot-spot with $dT=5$ K to the domain
349 (so that the domain mean SST is now larger than 300 K). We find that the speed of aggregation,
350 based on the aggregation index, is similar, and is determined to leading order by dT . This gives
351 us confidence that the hot-spot temperature anomaly is indeed the main control parameter, not its
352 absolute temperature.

353 Previous studies showed that the self-aggregation of convective clouds is sensitive to initial con-
354 ditions so that just by changing initial noises which are small compared to the initial condition, the
355 aggregation onset may delay or hasten. To check the robustness of our results regarding the timing
356 of the onset and the speed of aggregation, we ran two small ensembles of 5 members for $dT5R70$
357 and $dT5R80$ with homogenized radiation, using different initial noises. The ensemble simulations
358 show that the aggregation onset and speed do not vary significantly among the members, in partic-
359 ular the $R=80$ km simulations are all faster than the $R=70$ km. This suggests that the aggregation
360 speed is set mostly by the hot-spot forcing, and dependency on the initial conditions is small.

361 *b. Two-box model: Pulled or pushed aggregation ?*

362 Here we further investigate the mechanisms involved in the aggregation of the convection in
 363 the absence of radiative feedback (Figure 6). Given the potential importance of expansion and
 364 strengthening of the dry patch for the onset of convective aggregation (consistent with the dry-
 365 ing in Figure 6b), we will interpret the results in light of a conceptual, two-box model with a
 366 dry and a moist region, illustrated in Figure 7. In the moist region, there is upward motion in
 367 deep convection. In the dry region, there is subsidence and no deep convection (thus no latent
 368 heat release). Therefore, given the small horizontal gradients of temperature in the tropics (so-
 369 called weak temperature gradient approximation or WTG (Sobel et al. 2001)), to first order the
 370 temperature equation for a given pressure level (500 hPa in the following) yields:

$$\frac{\partial T}{\partial t} + \Gamma w^{dry} = Q_{rad} \quad (3)$$

$$\Rightarrow w^{dry} = \frac{Q_{rad} - \partial T / \partial t}{\Gamma}, \quad (4)$$

371 where w^{dry} is the (negative) subsidence velocity (m/s), Q_{rad} the (negative) radiative cooling (K/s),
 372 and

$$\Gamma = \frac{T}{\theta} \frac{d\theta}{dz} \quad (5)$$

373 the static stability (θ denotes potential temperature in K). At equilibrium (i.e. $\partial T / \partial t = 0$), there is
 374 a balance between subsidence warming and radiative cooling in the dry environment. We neverthe-
 375 less retain the temperature term $\partial T / \partial t$ in anticipation of w^{dry} that it may be important during the
 376 onset of self-aggregation, before equilibrium is reached. Recall that in these simulations without
 377 radiative feedback, the radiative cooling rates are homogenized in space, but is allowed to evolve
 378 in time.

379 As stated in the introduction for self-aggregation with radiative feedbacks, the stronger radiative
 380 cooling in dry regions compared to the moist regions causes further subsidence drying and gen-

erates a circulation that "pushes" the moisture towards the deep convection area (Figure 7). Thus self-aggregation is rather a self-confinement of moisture, as dry regions expand and strengthen, pushing the convection in a small part of the domain in our doubly-periodic geometry. In the hot-spot aggregation however, the hot-spot increases the convective instability and leads to deep convection localized over the hot-spot. Warmer and moister low level conditions over the hot spot increases the convective instability compare to the environment if we assume that the free troposphere temperature is horizontally homogeneous (Bretherton and Smolarkiewicz 1989). This generates a large-scale circulation with upward motion over the hot-spot and subsidence in its environment, yielding subsidence drying and convectively suppressed conditions in the region surrounding the hot-spot. The moisture is thus "pulled" in the convective region by the large-scale circulation induced by the convective instability over the hot-spot.

The aggregation may be separated into two different phases (Figure 6): the aggregation onset phase where dry regions expand and dry further, and the equilibrium phase when aggregation is well established and the simulation is statistically in equilibrium. The mechanisms which govern aggregation at each of these phases might be different (Muller and Held 2012). For instance, Wing and Emanuel (2014) find that in the onset phase, surface latent heat fluxes act as a positive feedback largely due to enhanced latent heat fluxes in the moist region, while in the equilibrium phase the aggregation is opposed by enhanced surface fluxes in dry regions. Previous studies using the SAM model with homogeneous SST show that the radiative feedback is necessary for both the onset and the maintenance of aggregation, so that homogenizing the radiation profile even after the formation of aggregation leads to a non-aggregated convection. We showed above that a persistent SST anomaly can generate and sustain aggregation even with homogenized radiation. In the following sections we further focus on the hot-spot simulations with homogenized radiation (Figure 6). We analyze first the aggregation processes by considering separately dry and moist

regions and by focusing on the aggregation onset phase. The equilibrium state will be addressed later in § 5. We define the onset phase as the time between the beginning of the simulation and the first maximum of the aggregation index. The onset phase varies from less than 10 days to more than 50 days for the simulations considered in Figure 6 and Table 1. Figure 6b shows that the aggregation index is mostly driven by the CRH values in the dry patches ($CRH < 25^{th}$ percentile).

c. *The aggregation onset phase*

The strength of the subsidence in the dry patch is characterized by its average vertical velocity at 500 hPa (\overline{W}_{500}^{dry}). Our hypothesis is that the subsidence strength is correlated with the aggregation onset and time scale. Stronger subsidence outside the hot-spot leads to an enhanced subsidence drying in dry regions, this is an important process that is mostly driven by the positive radiative feedback in the self-aggregation, but it is driven here only by the enhanced vertical motion over the hot-spot (Figure 7). Consistent with this hypothesis, at the beginning of the simulations, the subsidence over the dry patch is larger for larger hot-spots (Figure 8a). This can be interpreted as a very fast response to the convective activity over the hot-spot giving a strong subsidence over the surrounding cold ocean region. This response, much faster for larger hot-spots, is largely due to the fact that the initial conditions of the atmosphere (based on a SST of 300 K) enhanced the convective instability over the hot-spot. This plays a role in the aggregation speed, in a manner that may be exaggerated in regard to a hot-spot formation related, for example, to the diurnal surface temperature warming over an island. In that case, our results suggest that the adjustment is too slow (a few days) for such a diurnal variation to reach an equilibrium. Once the aggregation progresses, for hot-spot radius larger than 70 km, \overline{W}_{500}^{dry} becomes progressively weaker so that by the end of the aggregation onset phase, it becomes even weaker than for simulations without aggregation.

Equation 4 gives a good estimate of the evolution of the actual \overline{W}_{500}^{dry} (Figure 8b) that makes it possible to analyze further the contributions of the radiative cooling term Q_{rad} and of the warming term $\partial T / \partial t$ in the weakening of the subsidence over the dry patch (Figure 8c and 8d). The difference in the time evolution of the subsidence is largely controlled by the warming term $\partial T / \partial t$ and not by Q_{rad} during the aggregation onset phase. The warming term $\partial T / \partial t$ is large as the domain is adjusting to the warmer condition over the hot-spot. The adjusting time is about 10 days for large hot-spots. We note that this warming term is much smaller if we use atmospheric initial conditions corresponding to the hot-spot temperature. The larger temperature above the hot-spot yields warmer atmospheric temperatures there, which are progressively impressed on the whole domain through compensating subsidence and via propagating gravity waves (Bretherton and Smolarkiewicz 1989). As shown in Figure 8, this effect is stronger for larger hot-spots for which the term $\partial T / \partial t$ decreases dramatically during the aggregation onset phase. For large hot-spots, Q_{rad} is slightly larger at the end of the aggregation onset phase, showing the effect of a well organized dry patch compared to simulations without organized convection.

This moisture "pulling" leading to convective aggregation is associated to different overturning time scales in these simulations, with typically faster aggregation for larger hot-spots. Note however that for $R=285$ km, the subsidence is found to be slightly smaller compared to $R=180$ km or $R=220$ km, in good agreement with a longer aggregation onset phase (Figure 6). For $R=285$ km, the subsidence is smaller because the potential upward mass flux over the hot-spot is too large to be compensated by subsidence outside of the hot-spot, so that a relatively large part of the hot-spot is included in the subsiding region.

Thus, the aggregation is closely related to the large-scale circulation, as measured by the subsidence velocity in dry regions. The larger fractional area covered by the hot-spot the larger \overline{W}_{500}^{dry} . This can be well seen in Figure 8a.

452 The decrease of \overline{W}_{500}^{dry} during the aggregation onset phase for large hot-spots is caused by the
 453 initial transient warming (Equation 4 and Figure 8c). Eventually, \overline{W}_{500}^{dry} becomes nearly constant
 454 in time, as the equilibrium is reached. Then the main balance in dry regions is between subsidence
 455 warming and radiative cooling ($\partial T / \partial t \approx 0$). The warming-induced enhanced static stability (large
 456 Γ in Equation 4) reduces the subsidence velocity in aggregating simulations (Figure 8a). Thus the
 457 vertical subsiding velocities in dry regions of aggregated simulations become smaller than non-
 458 aggregating ones once equilibrium is reached. This is how the expansion and strengthening of the
 459 dry patch is halted and equilibrium is reached, despite the stronger radiative cooling rates. This
 460 equilibrium phase will be further analyzed in the following section.

461 **5. Equilibrium phase**

462 Here we investigate how the strongest convective cells and updrafts are distributed in the equi-
 463 librium phase, and whether the aggregated cluster stays over the hot spot. To study the equilibrium
 464 state, we consider a period of 15 days starting at day 35 and ending at day 50 for which the simu-
 465 lations already reached the equilibrium phase (Figure 6), except for hot-spot of R70 for which we
 466 look at the last five days as this period is closer to the equilibrium.

467 Figure 9 shows CRH and W_{500} fields averaged over this period. For $R \leq 65$ km, there is no
 468 aggregation visible on the CRH field or detected by aggregation index, however W_{500} is much
 469 stronger over the hot-spot compared to its environment. For $R = 70$ the aggregation is still on
 470 progress. The CRH map of this simulation shows both dry and moist area, however, similar to
 471 $R = 60$ and 65 , the convection over the hot-spot is much stronger than over the environment. For
 472 $R = 80$ km, the convection is not totally centered on the hot-spot for this equilibrium phase. For
 473 the largest hot-spots, the region of large CRH is well centered on the center of the hot-spots. The
 474 concentration of the moist patch over the hot-spot for aggregated simulations is not systematic.

475 In the simulations with interactive radiation (not homogenized in space), the aggregated cluster
 476 is indeed not always centered over the hot-spot (Figure 2.b). In fact, once equilibrium is reached
 477 in the simulations with radiative feedbacks, the moist patch seems to decouple from the surface.
 478 It does not stay in the same location and can move across the domain. Thus this result that the
 479 convection is located over the hot-spot is not robust once radiative feedbacks are accounted for.
 480 With radiative feedbacks, whether the convective cluster stays over the hot-spot probably depends
 481 on the strength of radiative feedbacks compared to the hot-spot effects.

482 Despite the large variability of the aggregation index and of the *CRH* pattern among the simu-
 483 lations without radiative feedbacks, maximum values of W_{500} are always located over the hot-spot
 484 (with an annular shape for $R \leq 65$ km) during the equilibrium phase (Fig.9). A striking result is
 485 that the fractional area of large W_{500} (e.g. $W_{500} > 0.08$ m/s) is relatively independent of the radius
 486 of the hot-spot. This region with large W_{500} (Figure 9b) has a fractional area of approximately 10
 487 % for all hot-spot radius.

488 Figure 10 shows the vertical profiles of the domain mean relative humidity and radiative cooling
 489 rates at equilibrium. Simulations with large aggregation index have a drier average profile in
 490 agreement with low *CRH* in the dry patch (Fig.6) and with earlier studies of self-aggregation.
 491 Average radiative cooling profiles are similar among the simulations which aggregate, with a large
 492 radiative cooling rate near the surface. These profiles are consistent with the very dry conditions
 493 and strong low-level radiative cooling accompanying aggregation found in earlier studies (Muller
 494 and Bony 2015).

495 6. Conclusions

496 In this paper, we investigate the role of persistent warm SST anomalies (hot-spots) on the ag-
 497 gregation of deep convective clouds in cloud-resolving simulations. To this end, we perform sim-

498 ulations in radiative-convective equilibrium with SST anomalies of varying size and amplitude,
499 but keeping the domain mean SST constant between simulations. Earlier studies with homoge-
500 neous SSTs find that radiative feedbacks are necessary for both the onset and maintenance of a
501 self-aggregation of the convection for typical tropical temperatures (~ 300 K). As for previous
502 studies, we find that self-aggregation over homogeneous SSTs is favored at warm temperatures.
503 We also find that the presence of a hot-spot significantly accelerates the aggregation process and
504 extends the range of average SSTs for which aggregation occurs.

505 We interpret these different behaviors by the fact that the mechanisms for convective aggregation
506 with a hot-spot or with homogeneous SSTs are different. With homogeneous SST, the aggregation
507 of convection starts by a strengthening and an expansion of a dry region. Strong radiative cooling
508 in dry regions yields enhanced subsidence that further dries the dry regions and that "pushes"
509 low-level moisture toward the convective region (Figure 7a). In other words, radiatively-driven
510 subsidence inhibits convection in the dry region (Wing et al. 2017; Bretherton et al. 2005; Muller
511 and Held 2012).

512 With a hot-spot, we find that aggregation (it is no more a self-aggregation since it is forced
513 by the persistent SST anomaly) can occur even in the absence of radiative feedbacks (removed
514 by homogenizing horizontally radiative cooling rates) if the hot-spot is warm and large enough.
515 The hot-spot triggers aggregation by locally increasing the convective instability. Indeed, the
516 warmer and moister conditions at low level over the hot-spot favor deep convection, which brings
517 the atmosphere towards a warmer condition. These warmer temperatures are imprinted over the
518 whole domain through compensating subsidence warming in drier regions and via the propagation
519 of gravity waves (Bretherton and Smolarkiewicz 1989). This subsidence favors further drying in
520 dry regions. This is the positive feedback responsible for the expansion and strengthening of dry

regions in hot-spot simulations that aggregate. In other words, the hot-spot "pulls" convection over itself, by generating a large-scale circulation with subsidence outside the hot-spot (Figure 7b).

In our simulations, planetary rotation is neglected so there is no limiting scale (beyond the dissipative scale) for the propagation of waves. So in our doubly-periodic geometry, the subsidence compensates upward convective motion and is thus potentially stronger when the fractional area of the hot-spot increases. In particular, for a given hot-spot radius, the subsidence is sensitive to the domain size. This highlights the importance of using large domains when investigating island convection in similar non-rotating doubly-periodic settings, in order to either avoid or control the triggering of self-aggregation feedbacks. In particular, the doubly-periodic confinement of the large scale circulation induced by surface heterogeneities may explain the non-monotonic responses of precipitation to an island found in idealized simulations of convection over tropical islands. In such simulations, precipitation is found to increase and then decrease as a function of island radius holding the domain size fixed. Our results suggest that the large-scale circulation induced by the island may be impacted by the domain size if the domain is not large enough compared to the island.

In reality, with planetary rotation, the scale of the large-scale circulation induced by SST anomalies is likely determined by the Rossby radius of deformation. Our results suggest that for a large enough fractional area of SST anomalies compared to this large-scale circulation, self-aggregation feedbacks could play a role in organizing deep convection over SST anomalies. In the ocean, SST anomalies of the size studied here ($\mathcal{O}(100 \text{ km})$) are not uncommon, taking the form of mesoscale eddies (Chelton 2011). Their contribution to convective organization deserves further investigation. Finally, these findings raise questions on the organization of deep convection over tropical islands, e.g. of the maritime continent. There, a strong diurnal cycle further interacts with aggregation feedbacks and tendencies (Cronin et al. (2014)). Our results show that the adjustment of

the average temperature profile to the hot-spot SST anomaly takes a few days for large hot-spots, which is very slow compared to diurnal variability of surface temperature over tropical islands (reaching to a maximum typically in 6h between sunrise and noon). Therefore, the atmosphere, and the convective aggregation pattern itself, will not have time to fully adjust before the island starts cooling down in the afternoon. Further work is needed to investigate the implication of our results on the diurnal cycle of convection over tropical islands.

Acknowledgments. This project has received funding from the Marie - Sklodowska Curie Actions (MSCA) under the European Union's Horizon 2020 research and innovation programme (grant agreement n675675). The authors gratefully acknowledge funding from the French national program Les Enveloppes Fluides et l'Environnement (LEFE) of Institut National des Sciences de l'Univers (INSU), and from the program Paris Sciences et Lettres PSL-NYU (ANR-10-IDEX-0001-02). Finally, the authors would like to thank Kerry Emanuel and two anonymous reviewers for their useful comments about this work.

References

- Abbot, D. S., 2014: Resolved snowball earth clouds. *J. Climate*, **27** (12), 4391–4402, doi:10.1175/JCLI-D-13-00738.1.
- Bellenger, H., J. Duvel, M. Lengaigne, and P. Levan, 2009: Impact of organized intraseasonal convective perturbations on the tropical circulation. *Geophys. Res. Lett.*, **36**, L16 703, doi:10.1029/2009GL039584.
- Beringer, J., and N. Tapper, 2002: Surface energy exchanges and interactions with thunderstorms during the maritime continent thunderstorm experiment (mctex). *J. Geophys. Res.*, **107** (D21), AAC 3–1–AAC 3–13, doi:10.1029/2001JD001431.

567 Bretherton, C. S., P. N. Blossey, and M. Khairoutdinov, 2005: An energy-balance analysis of
 568 deep convective self-aggregation above uniform SST. *J. Atmos. Sci.*, **62** (12), 4273–4292, doi:
 569 10.1175/JAS3614.1.

570 Bretherton, C. S., and P. K. Smolarkiewicz, 1989: Gravity waves, compensating subsidence
 571 and detrainment around cumulus clouds. *J. Atmos. Sci.*, **46** (6), 740–759, doi:10.1175/
 572 1520-0469(1989)046<0740:GWCSAD>2.0.CO;2.

573 Chelton, D., 2011: Global observations of nonlinear mesoscale eddies. *Prog. Oceanogr.*, **91** (2),
 574 167 – 216, doi:https://doi.org/10.1016/j.pocean.2011.01.002.

575 Collins, W. D., and Coauthors, 2006: The formulation and atmospheric simulation of the com-
 576 munity atmosphere model version 3 (cam3). *J. Climate*, **19** (11), 2144–2161, doi:10.1175/
 577 JCLI3760.1.

578 Coppin, D., and S. Bony, 2015: Physical mechanisms controlling the initiation of convective
 579 self-aggregation in a general circulation model. *J. Adv. Model. Earth Syst.*, **7** (4), 2060–2078,
 580 doi:10.1002/2015MS000571.

581 Cronin, T., K. A. Emanuel, and P. Molnar, 2014: Island precipitation enhancement and the diurnal
 582 cycle in radiative-convective equilibrium. *Quart. J. Roy. Meteor. Soc.*, **141**, doi:10.1002/qj.2443.

583 Crook, N. A., 2001: Understanding hector: The dynamics of island thunderstorms. *Mon. Wea.*
 584 *Rev.*, **129**, 1550–1563, doi:10.1175/1520-0493(2001)129<1550:UHTDOI>2.0.CO;2.

585 Daleu, C. L., R. S. Plant, and S. J. Woolnough, 2017: Using the weak-temperature gradient ap-
 586 proximation to evaluate parameterizations: An example of the transition from suppressed to
 587 active convection. *J. Adv. Model. Earth Syst.*, **9** (6), 2350–2367, doi:10.1002/2017MS000940.

588 Emanuel, K. A., A. A. Wing, and E. M. Vincent, 2014: Radiative-convective instability. *J. Adv.*
589 *Model. Earth Syst.*, **6** (1), 75–90, doi:10.1002/2013MS000270.

590 Grabowski, W. W., 2006: Impact of explicit atmosphereocean coupling on MJO-like coherent
591 structures in idealized aquaplanet simulations. *J. Atmos. Sci.*, **63** (9), 2289–2306, doi:10.1175/
592 JAS3740.1.

593 Grabowski, W. W., and M. W. Moncrieff, 2001: Large-scale organization of tropical convection
594 in two-dimensional explicit numerical simulations. *Quart. J. Roy. Meteor. Soc.*, **127** (572), 445–
595 468, doi:10.1002/qj.49712757211.

596 Gray, W., and R. Jacobson, 1977: Diurnal variation of deep cumulus convection. *Mon. Wea. Rev.*,
597 **105**, 1171–1187, doi:10.1175/1520-0493(1977)105<1171:DVODCC>2.0.CO;2.

598 Holloway, C. E., 2017: Convective aggregation in realistic convective-scale simulations. *J. Adv.*
599 *Model. Earth Syst.*, **9** (2), 1450–1472, doi:10.1002/2017MS000980.

600 Houze, R. A., Jr., 2004: Mesoscale convective systems. *Rev. Geophys.*, **42** (4), RG4003, doi:
601 10.1029/2004RG000150.

602 Khairoutdinov, M. F., and K. A. Emanuel, 2010: Aggregated convection and the regulation of
603 tropical climate. *Preprints, 29th conference on Hurricanes and Tropical Meteorology, Tucson,*
604 *AZ, Amer. Meteor. Soc.*, **P2.69**.

605 Khairoutdinov, M. F., and D. A. Randall, 2003: Cloud resolving modeling of the ARM summer
606 1997 IOP: Model formulation, results, uncertainties, and sensitivities. *J. Atmos. Sci.*, **60** (4),
607 607–625, doi:10.1175/1520-0469(2003)060<0607:CRMOTA>2.0.CO;2.

608 Kuang, Z., 2012: Weakly forced mock walker cells. *J. Atmos. Sci.*, **69**, 2759–2786, doi:10.1175/
609 JAS-D-11-0307.1.

610 Mapes, B., and R. Neale, 2011: Parameterizing convective organization to escape the entrainment
611 dilemma. *J. Adv. Model. Earth Syst.*, **3** (2), doi:10.1029/2011MS000042.

612 Mapes, B. E., 2001: Water's two height scales: The moist adiabat and the radiative troposphere.
613 *Quart. J. Roy. Meteor. Soc.*, **127** (577), 2353–2366, doi:10.1002/qj.49712757708.

614 Muller, C. J., 2013: Impact of convective organization on the response of tropical precipitation
615 extremes to warming. *J. Climate*, **26**, 5028–5043, doi:10.1175/JCLI-D-12-00655.1.

616 Muller, C. J., and S. Bony, 2015: What favors convective aggregation and why? *Geophys. Res.*
617 *Lett.*, **42** (13), 5626–5634, doi:10.1002/2015GL064260.

618 Muller, C. J., and I. M. Held, 2012: Detailed investigation of the self-aggregation of convection in
619 cloud-resolving simulations. *J. Atmos. Sci.*, **69**, 2551–2565, doi:10.1175/JAS-D-11-0257.1.

620 Muller, C. J., and P. A. O’Gorman, 2011: An energetic perspective on the regional response of
621 precipitation to climate change. *Nature Climate Change*, **1** (5), 266–271.

622 Muller, C. J., P. A. O’Gorman, and L. E. Back, 2011: Intensification of precipitation ex-
623 tremes with warming in a cloud-resolving model. *J. Climate*, **24** (11), 2784–2800, doi:
624 10.1175/2011JCLI3876.1.

625 Pauluis, O., and I. M. Held, 2002: Entropy budget of an atmosphere in radiative–convective equi-
626 librium. part i: Maximum work and frictional dissipation. *J. Atmos. Sci.*, **59** (2), 125–139, doi:
627 10.1175/1520-0469(2002)059<0140:EBOAAI>2.0.CO;2.

628 Qian, J.-H., 2008: Why precipitation is mostly concentrated over islands in the maritime continent.
629 *J. Atmos. Sci.*, **65** (4), 1428–1441, doi:10.1175/2007JAS2422.1.

630 Ramsay, H. A., and A. H. Sobel, 2011: Effects of relative and absolute sea surface temperature on
631 tropical cyclone potential intensity using a single-column model. *J. Climate*, **24** (1), 183–193,
632 doi:10.1175/2010JCLI3690.1.

633 Romps, D. M., 2010: A direct measure of entrainment. *J. Atmos. Sci.*, **67** (6), 1908–1927, doi:
634 10.1175/2010JAS3371.1.

635 Ruppert, J., and C. Hohenegger, 2018: Diurnal circulation adjustment and organized deep convec-
636 tion. *J. Climate*, doi:10.1175/JCLI-D-17-0693.1.

637 Sobel, A. H., and C. S. Bretherton, 2000: Modeling tropical precipitation in a single column. *J.*
638 *Climate*, **13** (24), 4378–4392, doi:10.1175/1520-0442(2000)013<4378:MTPIAS>2.0.CO;2.

639 Sobel, A. H., C. D. Burleyson, and S. E. Yuter, 2011: Rain on small tropical islands. *J. Geophys.*
640 *Res.*, **116** (D8), doi:10.1029/2010JD014695.

641 Sobel, A. H., J. Nilsson, and L. M. Polvani, 2001: The weak temperature gradient approximation
642 and balanced tropical moisture waves. *J. Atmos. Sci.*, **58**, 23, doi:10.1175/1520-0469(2001)
643 058<3650:TWTGAA>2.0.CO;2.

644 Sugimoto, S., K. Aono, and S. Fukui, 2017: Local atmospheric response to warm mesoscale ocean
645 eddies in the kuroshiooyashio confluence region. *Scientific Reports*, **7** (11871).

646 Tan, J., C. Jakob, W. B. Rossow, and G. Tselioudis, 2015: Increases in tropical rainfall driven
647 by changes in frequency of organized deep convection. *Nature*, **519** (7544), 451, doi:10.1038/
648 nature14339.

649 Tobin, I., S. Bony, and R. Roca, 2012: Observational evidence for relationships between the degree
650 of aggregation of deep convection, water vapor, surface fluxes, and radiation. *J. Climate*, **25**,
651 6885–6904, doi:10.1175/JCLI-D-11-00258.1.

652 Tompkins, A. M., 2001a: Organization of Tropical Convection in Low Vertical Wind Shears:
 653 The Role of Cold Pools. *J. Atmos. Sci.*, **58**, 16501672, doi:10.1175/1520-0469(2001)058<1650:
 654 OOTCIL>2.0.CO;2.

655 Tompkins, A. M., 2001b: Organization of tropical convection in low vertical wind shears: The
 656 role of water vapor. *J. Atmos. Sci.*, **58** (6), 529–545, doi:10.1175/1520-0469(2001)058<0529:
 657 OOTCIL>2.0.CO;2.

658 Tompkins, A. M., and G. C. Craig, 1998: Radiative-convective equilibrium in a three-
 659 dimensional cloud-ensemble model. *Quart. J. Roy. Meteor. Soc.*, **124**, 2073–2097, doi:10.1002/
 660 qj.49712455013.

661 Wang, S., and A. H. Sobel, 2011: Response of convection to relative sea surface temperature:
 662 Cloud-resolving simulations in two and three dimensions. *J. Geophys. Res.*, **116** (D11), doi:
 663 10.1029/2010JD015347.

664 Wang, S., and A. H. Sobel, 2017: Factors controlling rain on small tropical islands: Diurnal
 665 cycle, large-scale wind speed, and topography. *J. Atmos. Sci.*, **74** (11), 3515–3532, doi:10.1175/
 666 JAS-D-16-0344.1.

667 Wing, A., K. Emanuel, C. Holloway, and C. Muller, 2017: Convective self-aggregation
 668 in numerical simulations: A review. *Surv. Geophys.*, **38** (6), 1173–1197, doi:10.1007/
 669 978-3-319-77273-8_1.

670 Wing, A. A., and T. W. Cronin, 2016: Self-aggregation of convection in long channel geometry.
 671 *Quart. J. Roy. Meteor. Soc.*, **142** (694), 1–15, doi:10.1002/qj.2628.

672 Wing, A. A., and K. A. Emanuel, 2014: Physical mechanisms controlling self-aggregation of
673 convection in idealized numerical modeling simulations. *J. Adv. Model. Earth Syst.*, **6** (1), 59–
674 74, doi:10.1002/2013MS000269.

675 Zuidema, P., G. Torri, and C. Muller, 2017: Precipitation-induced atmospheric cold pools over
676 oceans and their interactions with the larger-scale environment. *Surv. Geophys.*, **38** (6), 1283–
677 1305, doi:10.1007/s10712-017-9447-x.

678 **LIST OF TABLES**

679	Table 1.	List of all the simulations with homogenized radiation. Shown are the hot-spot	
680		radius, the fractional area covered by it (with one digit for values below 10 %),	
681		its temperature anomaly (dT), ocean temperature and domain mean SST.	34

682 TABLE 1. List of all the simulations with homogenized radiation. Shown are the hot-spot radius, the fractional
683 area covered by it (with one digit for values below 10 %), its temperature anomaly (dT), ocean temperature and
684 domain mean SST.

HS Radius (km)	$A^{hs} / (A^{env} + A^{hs}) (\%)$	dT (K)	SST^{env} (K)	\overline{SST} (K)
60	3.4	5	299.83	300
65	4.0	5	299.80	300
70	4.6	5	299.77	300
80	6.1	5	299.69	300
80	6.1	3	299.81	300
180	31	5	298.46	300
220	46	5	297.70	300
285	77	5	296.15	300

685	LIST OF FIGURES	
686	Fig. 1.	Snapshots of near-surface air temperature (colors, K) and cloud water (grey shades) from two simulations with a hot-spot in the center of the domain (circle) for (a) a domain size 96*96km ² and (b) 288*288 km ² . (c) Time evolution of the aggregation index for those two simulations. 36
687		
688		
689		
690	Fig. 2.	Snapshots of <i>CRH</i> for simulations with (a) a uniform surface temperature and (b) a hot-spot with a SST anomaly of 5 K and a radius of 60 km. The black circle shows the hot-spot boundary. For both simulations the domain average SST is 300K and the domain size is 576*576 km ² 37
691		
692		
693		
694	Fig. 3.	Time evolution of the aggregation index for simulations with full radiative feedback for: (a) simulations with a uniform surface temperature (referred to as “Ocean” see §2b for a detailed description of the simulations); (b) simulations with a hot-spot of different sizes and SST anomalies. 38
695		
696		
697		
698	Fig. 4.	θv anomaly averaged over the boundary layer (from surface to 1000 m) for a) day 31 of ocean experiment at 300 K, b) day 11 of Hot-spot experiment dT5R60 and mean SST=300 K. 39
699		
700		
701	Fig. 5.	Snapshots of <i>CRH</i> for hot-spot simulations with homogenized radiation for: (a) SST anomaly of 5 K and a radius of 60 km and (b) SST anomaly of 5 K and a radius of 70 km. The black circle shows the hot-spot boundary. For both simulations, the domain average SST is 300 K and the domain size is 576*576 km ² 40
702		
703		
704		
705	Fig. 6.	Time evolution of (a) the aggregation index and (b) <i>CRH</i> averaged over driest quartile for different hot-spot radius for simulations with homogenized radiation. All the simulations have a domain size of 576*576 km ² and a hot-spot SST anomaly of 5 K except for one simulation with a radius of 80 km and a SST anomaly of 3 K. 41
706		
707		
708		
709	Fig. 7.	Schematic two-box model representing either a self-aggregation by radiative feedbacks or an aggregation forced by a hot-spot induced circulation. (a) Self-aggregation by radiative feedbacks is caused by a progressive expansion of a dry subsidence region under the effect of a strong radiative cooling, “pushing” the low-level moisture toward a constricted moist and warm convective region. (b) The aggregation is due to the large-scale circulation induced by the hot-spot persistent SST anomaly, “pulling” the moisture toward the warm anomaly. 42
710		
711		
712		
713		
714		
715	Fig. 8.	Time evolution of atmospheric parameters at 500 hPa averaged over the dry patch for different hot-spot sizes: (a) vertical velocity; (b) the right hand side of Equation 4; c) the time derivative of temperature and; (d) radiative cooling. The domain average SST is 300 K and the domain size is 576*576 km ² 43
716		
717		
718		
719	Fig. 9.	(top) <i>CRH</i> and (bottom) <i>W500</i> (m/s) averaged between day 35 and day 50 of the simulation for hot-spot of different sizes. The domain average SST is 300K, the hot-spot SST anomaly is 5 K and the domain size is 576*576 km ² . The black circle shows the hot-spot. 44
720		
721		
722	Fig. 10.	Domain average vertical profiles averaged between day 35 and day 50 of the simulation for hot-spot of different sizes. The domain average SST is 300 K, the hot-spot SST anomaly is 5 K and the domain size is 576*576 km ² 45
723		
724		

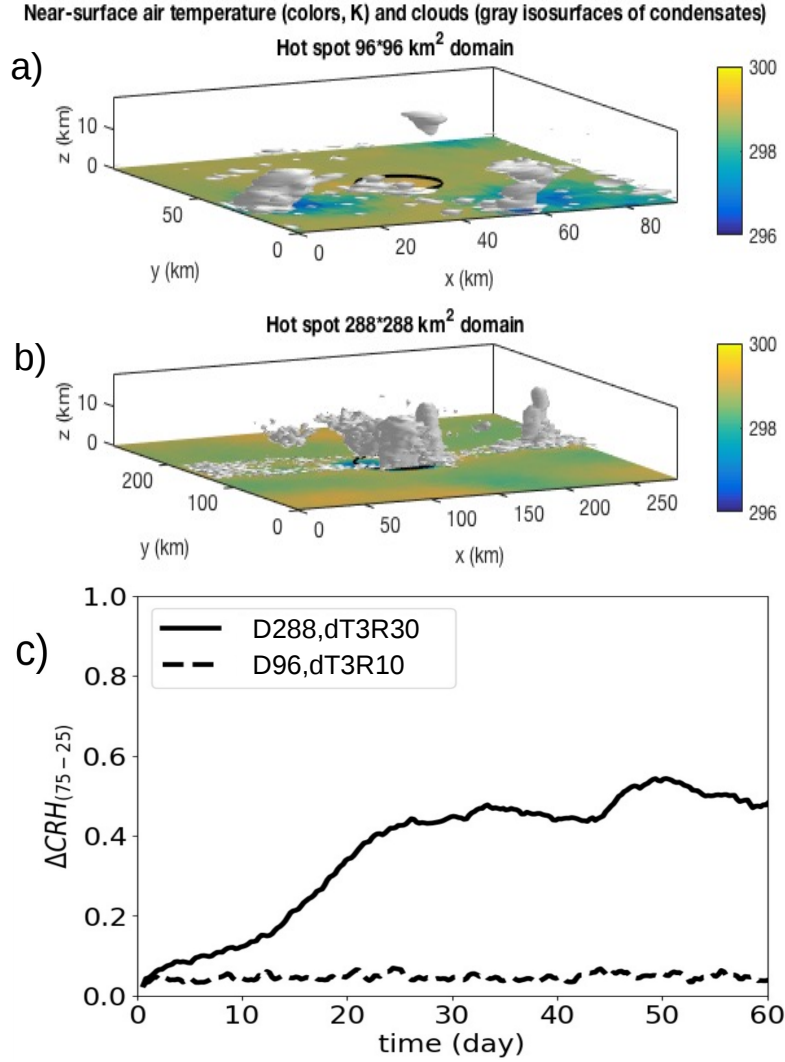


FIG. 1. Snapshots of near-surface air temperature (colors, K) and cloud water (grey shades) from two simulations with a hot-spot in the center of the domain (circle) for (a) a domain size 96*96km² and (b) 288*288 km². (c) Time evolution of the aggregation index for those two simulations.

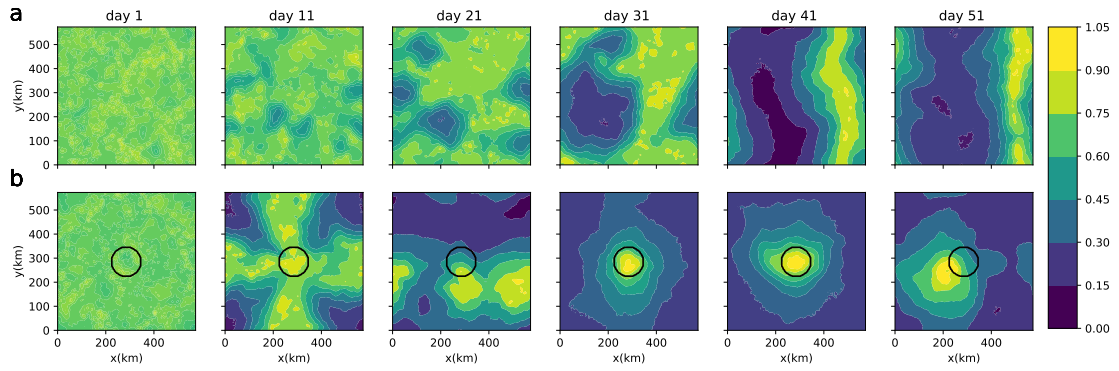


FIG. 2. Snapshots of *CRH* for simulations with (a) a uniform surface temperature and (b) a hot-spot with a SST anomaly of 5 K and a radius of 60 km. The black circle shows the hot-spot boundary. For both simulations the domain average SST is 300K and the domain size is $576 \times 576 \text{ km}^2$

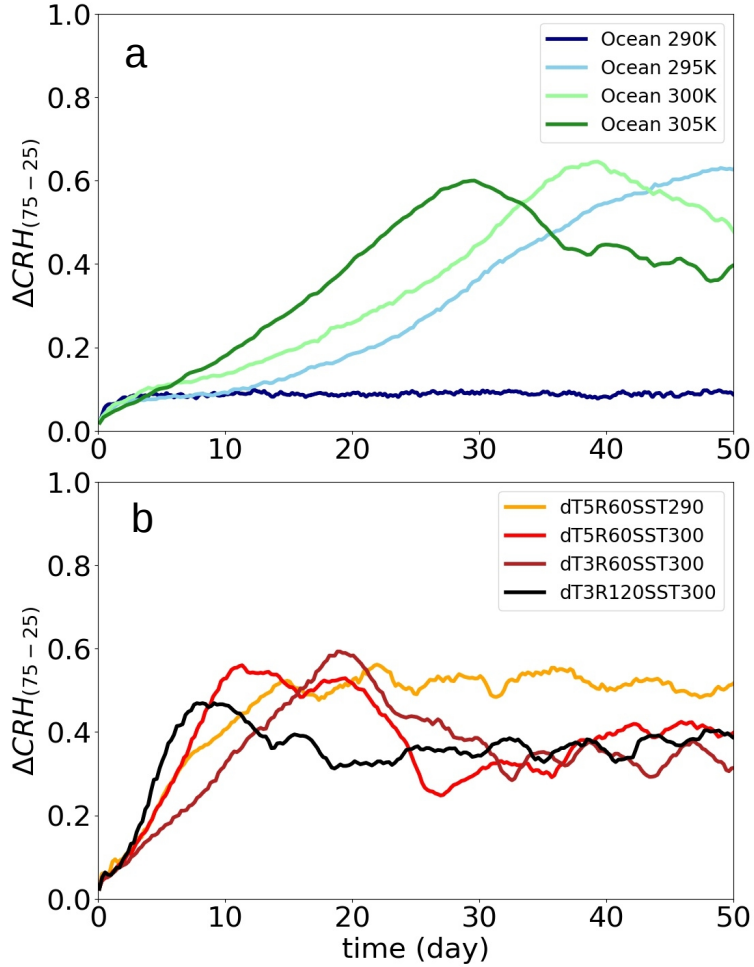


FIG. 3. Time evolution of the aggregation index for simulations with full radiative feedback for: (a) simulations with a uniform surface temperature (referred to as “Ocean” see §2b for a detailed description of the simulations); (b) simulations with a hot-spot of different sizes and SST anomalies.

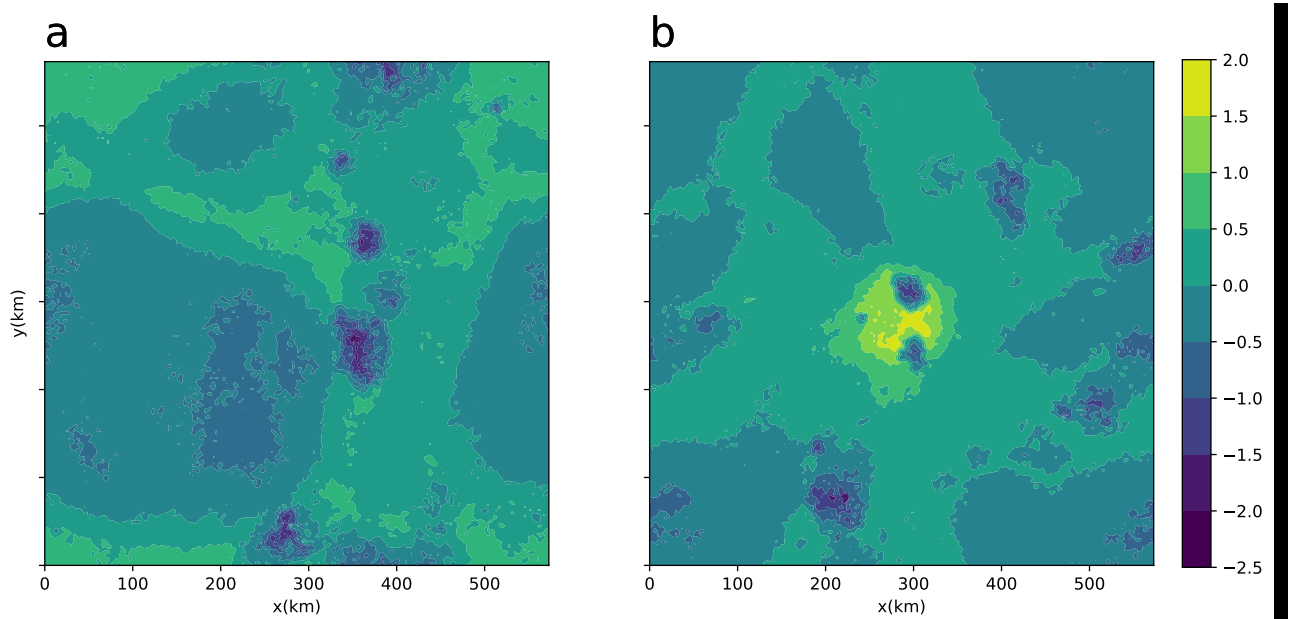
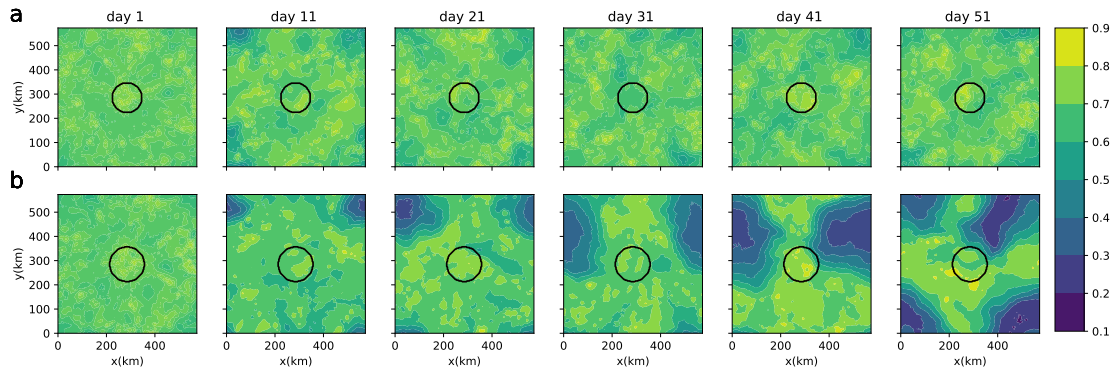


FIG. 4. θ_v anomaly averaged over the boundary layer (from surface to 1000 m) for a) day 31 of ocean
 experiment at 300 K , b) day 11 of Hot-spot experiment dT5R60 and mean SST=300 K.



736 FIG. 5. Snapshots of *CRH* for hot-spot simulations with homogenized radiation for: (a) SST anomaly of 5 K
 737 and a radius of 60 km and (b) SST anomaly of 5 K and a radius of 70 km. The black circle shows the hot-spot
 738 boundary. For both simulations, the domain average SST is 300 K and the domain size is $576 \times 576 \text{ km}^2$.

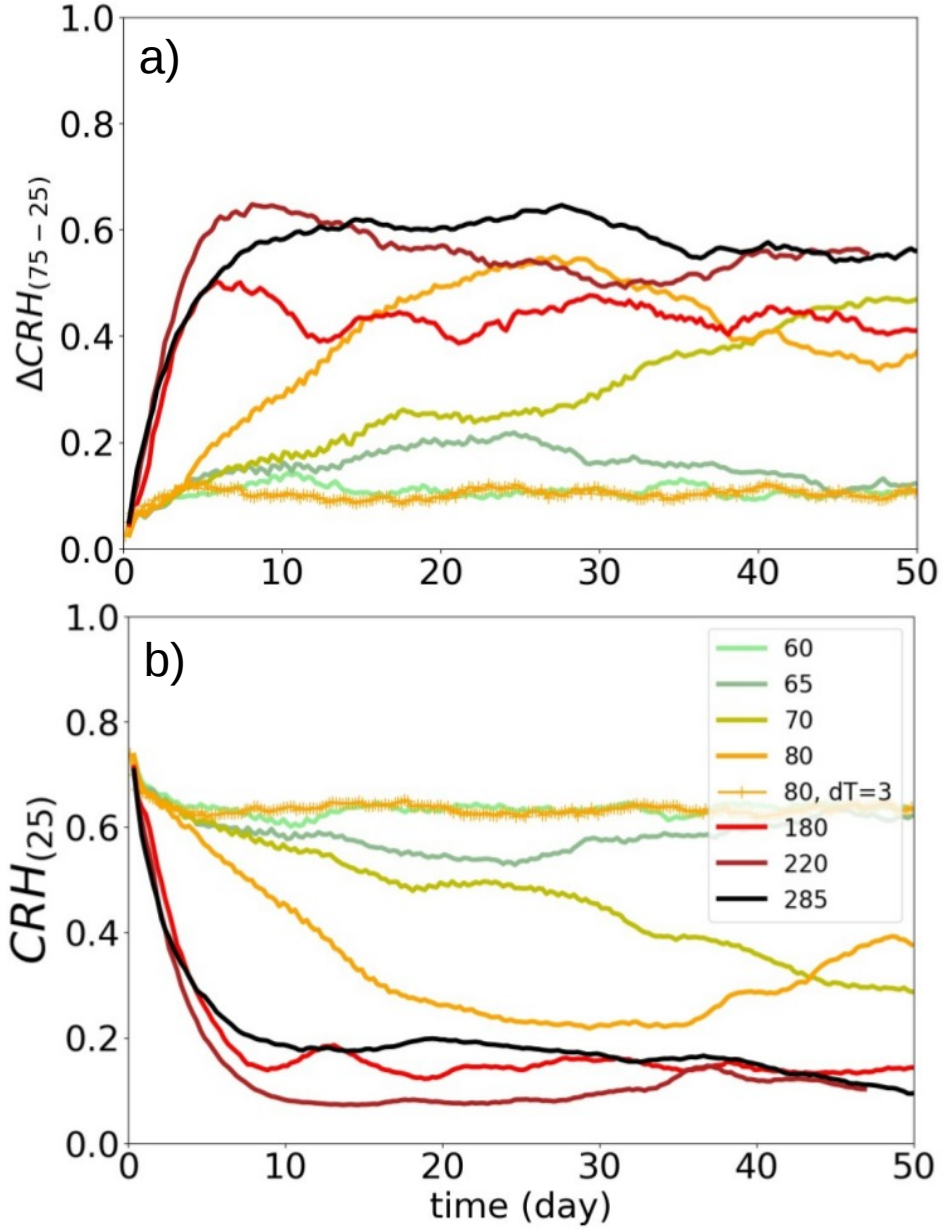


FIG. 6. Time evolution of (a) the aggregation index and (b) CRH averaged over driest quartile for different hot-spot radius for simulations with homogenized radiation. All the simulations have a domain size of 576×576 km² and a hot-spot SST anomaly of 5 K except for one simulation with a radius of 80 km and a SST anomaly of 3 K.

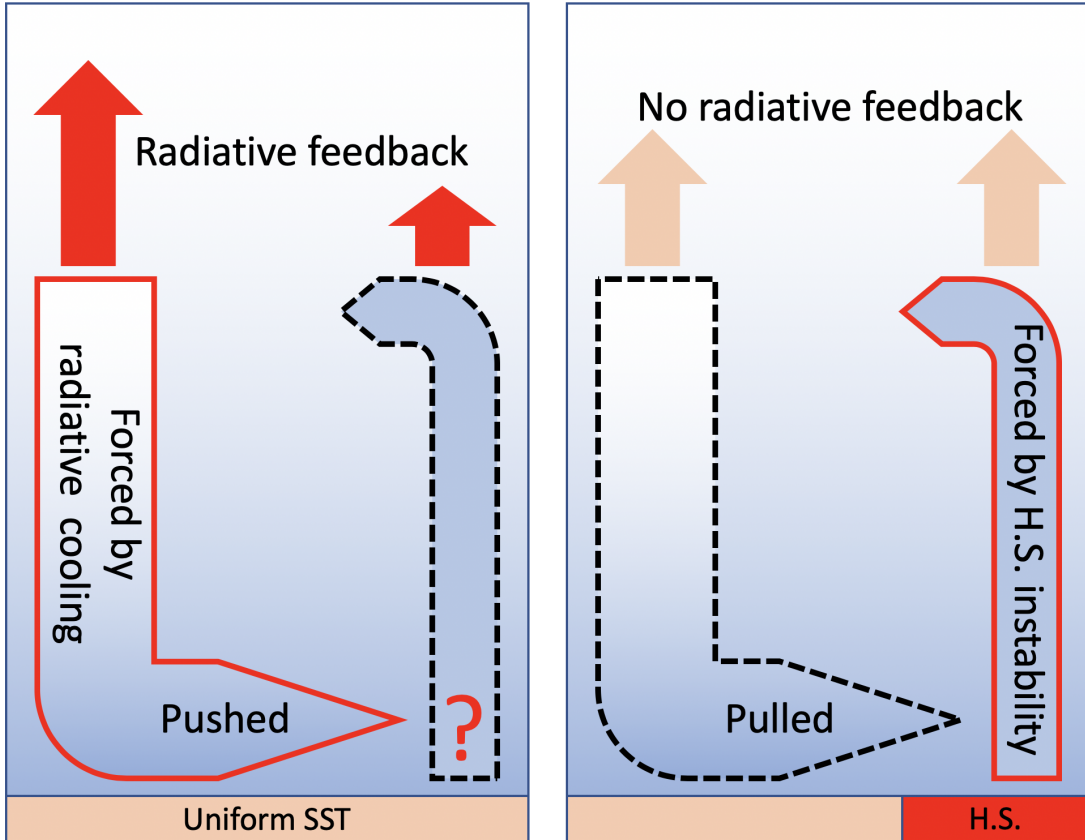


FIG. 7. Schematic two-box model representing either a self-aggregation by radiative feedbacks or an aggregation forced by a hot-spot induced circulation. (a) Self-aggregation by radiative feedbacks is caused by a progressive expansion of a dry subsidence region under the effect of a strong radiative cooling, "pushing" the low-level moisture toward a constricted moist and warm convective region. (b) The aggregation is due to the large-scale circulation induced by the hot-spot persistent SST anomaly, "pulling" the moisture toward the warm anomaly.

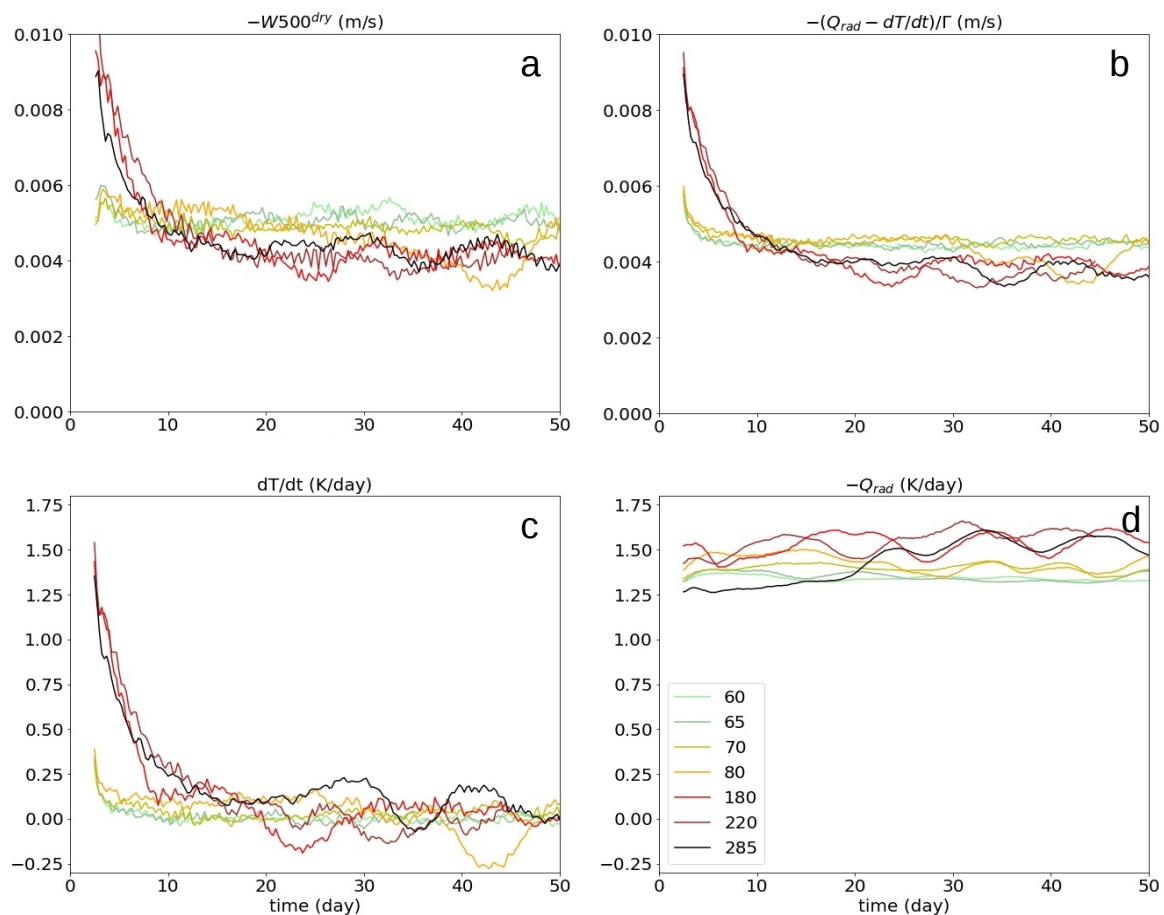
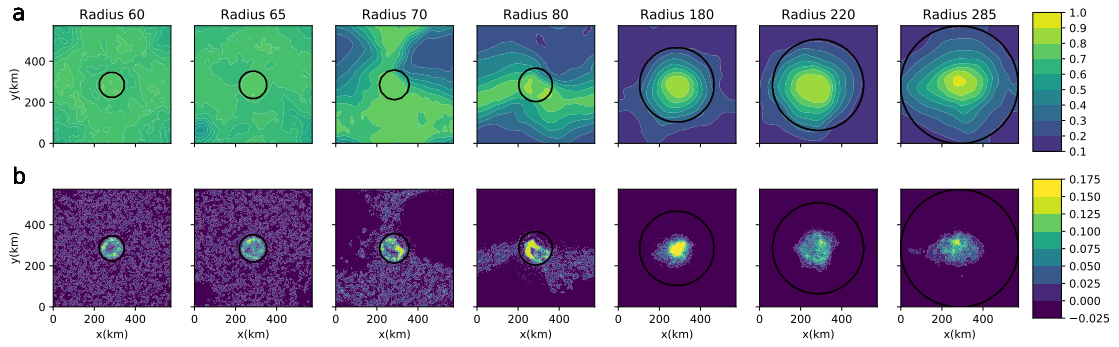


FIG. 8. Time evolution of atmospheric parameters at 500 hPa averaged over the dry patch for different hot-spot sizes: (a) vertical velocity; (b) the right hand side of Equation 4; (c) the time derivative of temperature and; (d) radiative cooling. The domain average SST is 300 K and the domain size is 576*576 km².



752 FIG. 9. (top) *CRH* and (bottom) *W500* (m/s) averaged between day 35 and day 50 of the simulation for hot-
 753 spot of different sizes. The domain average SST is 300K, the hot-spot SST anomaly is 5 K and the domain size
 754 is 576*576 km². The black circle shows the hot-spot.

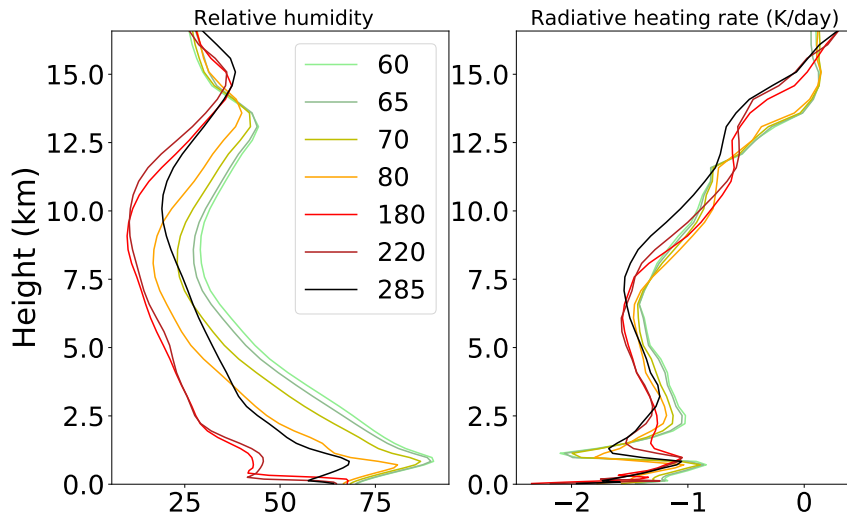


FIG. 10. Domain average vertical profiles averaged between day 35 and day 50 of the simulation for hot-spot of different sizes. The domain average SST is 300 K, the hot-spot SST anomaly is 5 K and the domain size is $576*576 \text{ km}^2$.